Talanta 141 (2015) 247–252

Contents lists available at ScienceDirect

Talanta

journal homepage: www.elsevier.com/locate/talanta

Label-free aptamer biosensor for thrombin detection based on functionalized graphene nanocomposites

Qingqing Wang [a,b], Zhixue Zhou [b], Yanling Zhai [b], Lingling Zhang [b], Wei Hong [b], Zhiquan Zhang [a,*], Shaojun Dong [b,*]

[a] College of Chemistry, Jilin University, Changchun 130012, PR China
[b] State Key Laboratory of Electroanalytical Chemistry, Changchun Institute of Applied Chemistry, Chinese Academy of Sciences, Changchun, Jilin 130022, PR China

ARTICLE INFO

Article history:
Received 16 December 2014
Received in revised form
1 April 2015
Accepted 5 April 2015
Available online 13 April 2015

Keywords:
Thrombin
Aptasensor
Impedance spectroscopy
Graphene
Nanocomposite

ABSTRACT

A label-free and amplified electrochemical impedimetric aptasensor based on functionalized graphene nanocomposites (rGO–AuNPs) was developed for the detection of thrombin, which played a vital role in thrombosis and hemostasis. The thiolated aptamer and dithiothreitol (TBA15–DTT) were firstly immobilized on the gold electrode to capture the thrombin molecules, and then aptamer functionalized graphene nanocomposites (rGO–TBA29) were used to fabricate a sandwich sensing platform for amplifying the impedimetric signals. As numerous negative charges of TBA29 on the electrode repelled to the $[Fe(CN)_6]^{4-/3-}$ anions, resulting in an obvious amplified charge-transfer resistance (R_{ct}) signal. The R_{ct} increase was linearly proportional to the thrombin concentration from 0.3 to 50 nM and a detection limit of 0.01 nM thrombin was achieved. In addition, graphene could also be labeled with other probes via electrostatic or π–π stacking interactions to produce signals, therefore different detection methods expanding wide application could be used in this model.

1. Introduction

Graphene has been a new star for application in various fields, such as catalysis [1], energy storage [2] and electrochemical biosensors [3] since its discovery in 2004. The applications of graphene in biosensors are focused on several fields. First, graphene or functionalized graphene has been used to modify the substrate such as GCE [4–6], ITO device [7], and quartz chip [8] because of their excellent conductivity and high chemical stability. Then graphene or graphene oxide can also act as a quencher to quench the fluorescence of illuminant for its unique electronic properties [9–11]. Li and his coworkers have realized real-time target monitoring in living cells by graphene oxide [10]. Last but not the least, graphene has high surface area; more and more graphene-based nanocomposites with different kinds of functions as enhanced sensing material have been reported [7,12,13].

Aptamers, which are singled-stranded oligonucleotides, possess high recognition ability to specific targets ranging from small inorganic, organic molecules even to proteins, cells or mycotoxins [14–16]. Since systematic evolution of ligands by an exponential enrichment (SELEX) process was firstly reported by Tuerk and Gold [17], various advanced methods for obtaining the aptamers have been developed. Aptamers exhibit multifarious advantages such as easy production, excellent controllability and versatility over the traditional recognition elements [18–22]. As a result, many aptamer-based methods have been used for the detection of proteins including quartz crystal microbalance (QCM) [23–25], surface plasmon resonance (SPR) [23,26], fluorescence [27,28], colorimetry [29], electrochemiluminescence (ECL) [30,31], electrochemistry [32,33], and so on. Among them, electrochemistry aptasensors have been widely used in medical, biological and environmental analyses. Especially, label-free electrochemical aptasensors have been developed rapidly due to their simplicity, convenience, low cost, etc. [34–36].

Here, we describe a label-free electrochemical impedimetric aptasensor for the determination of thrombin based on graphene–gold nanoparticle hybrids with enhanced sensitivity and selectivity for the aptasensors. Thrombin (TB), which plays a vital role in thrombosis and hemostasis [37], was chosen as a model protein in this work. And high sensitive detection of TB is essential for diagnosis. Because one TB molecule has two active sites for its aptamers (TBA15 and TBA29) [38], an electrode-TBA15/TB/TBA29-functionalized graphene nanocomposites sandwich system was fabricated as the sensing platform. With the aim to offer a significant amplification for the impedimetric detection of TB, reduced graphene oxide with gold nanoparticles (rGO–AuNPs) was used as a signal enhancer by covalently binding

* Corresponding authors. Tel.: +86 431 85692886; fax: +86 431 85689711.
E-mail addresses: zzq@jlu.edu.cn (Z. Zhang), dongsj@ciac.ac.cn (S. Dong).

http://dx.doi.org/10.1016/j.talanta.2015.04.012
0039-9140/

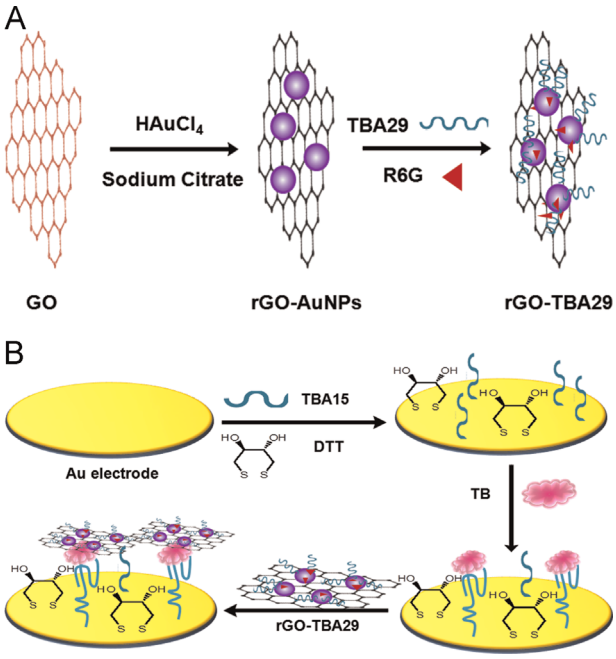

Fig. 1. (A) Illustration of the procedure for preparing rGO–AuNPs and rGO–TBA29 hybrid materials. (B) Schematic illustration of the impedimetric aptasensor with rGO–AuNPs as a signal amplified platform.

TBA29. For preparation, TBA15 and dithiothreitol (TBA15–DTT) were firstly immobilized on the gold electrode, followed by capturing the target TB, then the TBA29 functionalized reduced graphene oxide (rGO–TBA29) could further bind to TB to form a sandwich sensing system on the electrode as shown in Fig. 1. By using an electrochemical impedance spectroscopy (EIS) method, an efficient amplified charge-transfer resistance (R_{ct}) was obtained because hundreds of negatively assembled TBA29 repelled the $[Fe(CN)_6]^{4-/3-}$ anions. This approach not only presents a simple and general model for signal amplification of the impedimetric sensor but also offers a promising signal amplified model for protein detection. Because graphene could be labeled with other probes via electrostatic or π–π stacking interactions to produce signals, this model could also apply to other different methods such as SPR, ECL and so on. As a result, this aptasensor provides a very sensitive and promising detection model in the field of bioassay.

2. Experimental

2.1. Materials and chemicals

Graphene oxide (GO) was synthesized from natural graphite powder by a modified Hummers method [39]. Dithiothreitol (DTT) was obtained from Sigma-Aldrich. Tris(2-carboxyethyl)phosphine hydrochloride (TCEP) was bought from Bio Basic Inc. (Markham Ontario, Canada). Rhodamine6G (R6G) was obtained from Fluka (Buchs, Switzerland). Chloroauric acid ($HAuCl_4 \cdot 4H_2O$) and Tris (hydroxymethyl)aminomethane (Tris) were purchased from Shanghai Chemical Reagent Company (Shanghai, China). All other chemicals were of analytical grade. Ultrapure water was used throughout the study.

Thiolated thrombin aptamers TBA15 (5′-HS-SH-$(CH_2)_6$-TTT TTT TTG GTT GGT GTG GTT GG-3′) and TBA29 (5′-HS-$(CH_2)_6$-TTT TTT TTA GTC CGT GGT AGG GCA GGT TGG GGT GAC T) were synthesized by Sangon Biotech Co. Ltd. (Shanghai, China). Thrombin, bovine serum albumin (BSA), Trypsin, immunoglobulin G (IgG) were obtained from Sigma-Aldrich. The proteins and DNA were prepared in 34 mM Tris–HCl buffer (pH 7.4, 233 mM NaCl, 8.5 mM KCl and 3.4 mM $MgCl_2$) and stored at 4 °C before use.

2.2. Apparatus

EIS measurement was performed on a Zahner Zennium electrochemical workstation (ZAHNER-Elektrik GmbH & Co.KG, Germany) and CV measurement was performed with a model CH Instrument 832B electrochemical workstation (Shanghai Chenhua Equipments, China). A conventional three electrode electrochemical cell was used here with a Ag–AgCl reference electrode, a bare gold electrode (1.2 mm in diameter) as a working electrode and a platinum wire as a counter electrode. Both EIS and CV measurements were carried out at room temperature in the solution of 5 mM $K_4[Fe(CN)_6]/K_3[Fe(CN)_6]$ in Tris–HCl buffer, and EIS was performed under an oscillation potential of 5 mV over the frequency range of 1 MHz to 0.1 Hz. High-resolution transmission electron microscopy (HRTEM) measurements were performed on a JEM-2100F high-resolution transmission electron microscope operating at 200 kV. Transmission electron microscopy (TEM) was performed on a HITACHI H-600 Analytical TEM with an accelerating voltage of 100 kV. X-ray photoelectron spectroscopy (XPS) measurement was performed on an ESCALAB-MKII spectrometer (VG Co., United Kingdom) with Al Kα X-ray radiation as the X-ray source for excitation.

2.3. Synthesis of rGO–AuNPs

The rGO–AuNPs material was synthesized in a one-pot reaction according to the reported literature [40]. Briefly, 60 mg of sodium citrate was added to homogeneous GO dispersion (50 mL, 0.1 mg mL^{-1}) under refluxing and stirring. The mixture was further refluxed and stirred for 2.5 h, whereupon 100 μL $HAuCl_4$ (2 wt% in water) was quickly added to the above solution and reflux was continued for another 30 min. Finally, the resulting homogeneous black rGO–AuNPs dispersion was centrifuged at 12,000 rpm and washed with water. Subsequently, the material was redispersed into 6 mL water by sonication for further use.

2.4. Preparation of rGO–TBA29

The TBA29 functionalized reduced graphene oxide was prepared according to the procedure of literature [41] with a little modification. Detailedly, 20 μL of TCEP (1 mM in water) and excess of TBA29 was added to 100 μL of as-prepared rGO–AuNPs suspension and incubated for 24 h before diluting to 0.5 mL with water. After centrifugation at 12,000 rpm for 10 min twice to remove the free DNA, 100 μL of 0.1 mM R6G used to block the remained space of rGO–AuNPs surface was added to the above mixture overnight. Then rinsed with water again and stored the mixture at 4 °C before use.

2.5. Fabrication of the aptasensor

Prior to aptamer immobilization, the gold electrode (1.2 mm in diameter) was polished with 1.0 and 0.3 μm alumina slurry respectively, and ultrasonically washed with water, ethanol and water. Then the electrode was electrochemically cleaned in 0.1 M H_2SO_4 by potential scanning between −0.2 and 1.6 V until a reproducible cyclic voltammetry was obtained. Finally, the electrode was rinsed thoroughly with water and dried under nitrogen gas.

For immobilization of the aptamer, 10 μL of TBA15 solution (5 μM with 200 μM DTT in Tris–HCl buffer) was placed on the cleaned gold electrode with a plastic cap overnight (about 10 h) at room temperature. Then, Au/TBA15–DTT interface was immobilized with 10 μL concentration of TB respectively, or 1 μM non-

specific protein (trypsin, IgG and BSA) for 90 min in control experiment. Subsequently, 10 μL of rGO–TBA29 was coated on the Au/TBA15–DTT/TB electrode for another 5 h to obtain a sandwich sensing system. After each step, the electrode was washed with water for several times and dried in a nitrogen stream.

3. Results and discussion

3.1. Preparation and characterization of rGO–AuNPs nanocomposites

For synthesis of rGO–AuNPs, we chose a simple method using sodium citrate as a reducing reagent. Here, sodium citrate stabilized rGO through strong hydrogen bonding interactions, also acted as a protecting agent giving uniform AuNPs. With refluxing and stirring for only three hours in all, the mixture of GO and $HAuCl_4$ was reduced by sodium citrate at the same time forming a stable dark dispersion in water. The dispersion was homogeneous and no visible precipitate was observed over a period of months.

TEM images of GO (Fig. 2A) and rGO–AuNPs (Fig. 2B and C) were direct evidence for the successful immobilization of AuNPs onto the rGO surface. As shown in Fig. 2, the as-prepared rGO–AuNPs had a rougher surface than the GO, which indicated that a large number of AuNPs had been successfully absorbed on the surface of rGO. And the diameter of AuNPs was about 7.5 nm. It could also be seen that small AuNPs were uniformly and densely dispersed on the rGO surface, which would provide tremendous binding sites for TBA29. In addition, free AuNPs could hardly be observed outside the rGO surface, indicating that all AuNPs were well absorbed on the surface of rGO.

XPS was performed to further confirm the reduction of GO and AuNPs formation. Fig. 3 displayed the high-resolution of C 1s XPS spectrum of GO samples. There were three types of carbon peaks centered at 284.6, 286.7 and 288.5 eV, corresponding to C–C, C–O and C=O groups, respectively. The peak intensity of C–O was high in GO (Fig. 3A), which obviously decreased in rGO–AuNPs (Fig. 3B) after the reducing process, indicating that GO was reduced successfully. Furthermore, a pair of doublet peaks of Au 4f at 84.0 and 87.7 eV were both observed in Fig. 3C, which confirmed that Au existed in rGO–AuNPs and the rGO–AuNPs nanocomposites were synthesized successfully.

3.2. Design of the aptasensor

As illustrated in Fig. 1, a typical sandwich aptasensor based on the signal amplification was designed for TB. TBA15 with DTT was first immobilized on the gold electrode surface via the self-assembly and then the as-prepared functional sensing interface was incubated with a series of TB solutions respectively for detection. The rGO–TBA29 was subsequently bound to the resulting electrode forming a sandwich system. The properties of bare electrode, Au/TBA15–DTT, Au/TBA15–DTT/TB, and Au/TBA15-DTT/TB/rGO–TBA29 were investigated by both CV and EIS measurements exploiting the solution based on redox probe $[Fe(CN)_6]^{3-/4-}$. As shown in Fig. 4A, the semicircle portion obtained at high frequencies corresponded to the electron transfer limiting process. And the semicircle diameter can be directly regarded as the R_{ct} value. The R_{ct} value increased obviously when TBA15 was modified on the electrode surface due to electrostatic repulsion between negatively charged TBA15 and $[Fe(CN)_6]^{3-/4-}$ in solution [42]. R_{ct} decreased to 1286 Ω for TBA15–DTT binary layer because DTT could be used to displace nonspecific interactions between TBA15 and electrode surface and benefits for TBA15 standing up from the surface [43], which displayed low background for TB detection. Owing to the bulky TB molecules blocking the electrode surface, R_{ct} increased obviously when TB was captured. Followed by the conjugation of rGO–TBA29 (Fig. 4B) to form a sandwich system, a further enhancement of R_{ct} value was

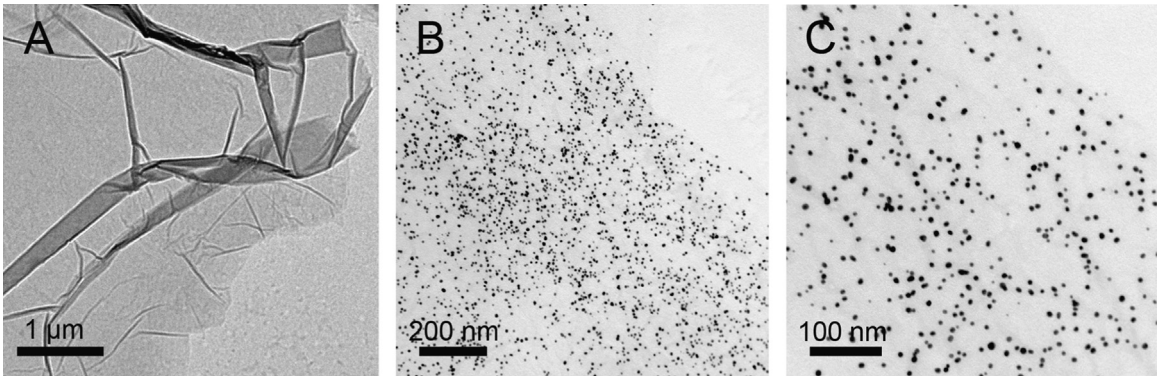

Fig. 2. HRTEM image of GO (A) and TEM images of rGO–AuNPs at low (B) and high (C) magnification.

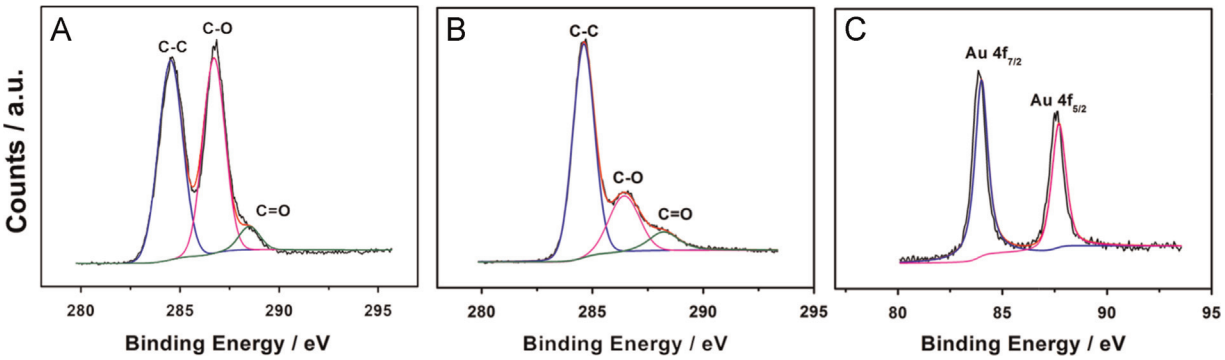

Fig. 3. C 1s XPS spectra of GO (A) and rGO–AuNPs (B), Au 4f XPS spectra of rGO–AuNPs (C).

reached (from 9938 Ω to 14,920 Ω). As a large number of AuNPs were absorbed on the surface of rGO, hundreds of TBA29 could bind to the AuNPs surface covalently through the Au–S linkage, which contributed to the dramatic enhancement of R_{ct} value. As a result, an amplified impedimetric aptasensor with rGO–TBA29 for the detection of TB was obtained. And the CV responses in Fig. 4B were in agreement with the EIS.

3.3. EIS detection in the presence of TB

For TB detection, the as-prepared sensing interface was immobilized with a series of TB solutions for 90 min. Then the functional material rGO–TBA29 was coated on the electrode surface for several hours. The binding time of rGO–TBA29 was investigated as shown in Fig. 5A, the R_{ct} value of Au/TBA15–DTT/TB/rGO–TBA29 obviously increased with increasing time and it reached a plateau at about 5 h, and thus we chose 5 h as the incubation time in the following experiments.

Fig. 5B and C showed the Nyquist plots of faradic impedance spectra of the aptasensor for different concentrations of TB in buffer. The inset in Fig. 5C showed the circuit that includes the common existing electrolyte resistance (R_s), Warburg impedance (Z_w), double-layer capacitance (C_d) and the charge-transfer resistance (R_{ct}) [44]. Among them, R_{ct} is the most directive parameter for the changes on the electrode interface [45]. As can be seen, with increasing concentration of TB, the EIS signals were increased obviously indicating that the aptasensor possessed high sensitivity to TB. And R_{ct} had a fine linear relationship with the concentration of TB from 0.3 nM to 50 nM (Fig. 5D). The regression equation was R_{ct} (Ω)=587.9C_{TB} (nM)+2079, and the detection limit was as low

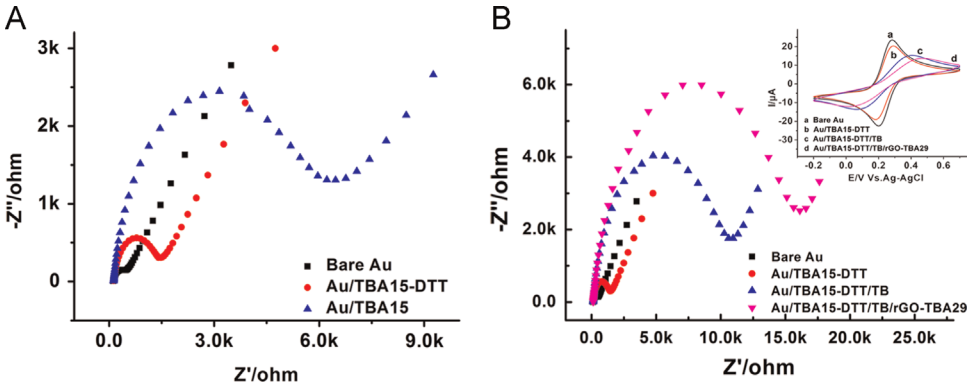

Fig. 4. (A) Comparison of TBA15 and TBA15–DTT modified the bare Au electrode. (B) EIS and CV responses of different sensing interfaces. The concentration of TB was 20 nM.

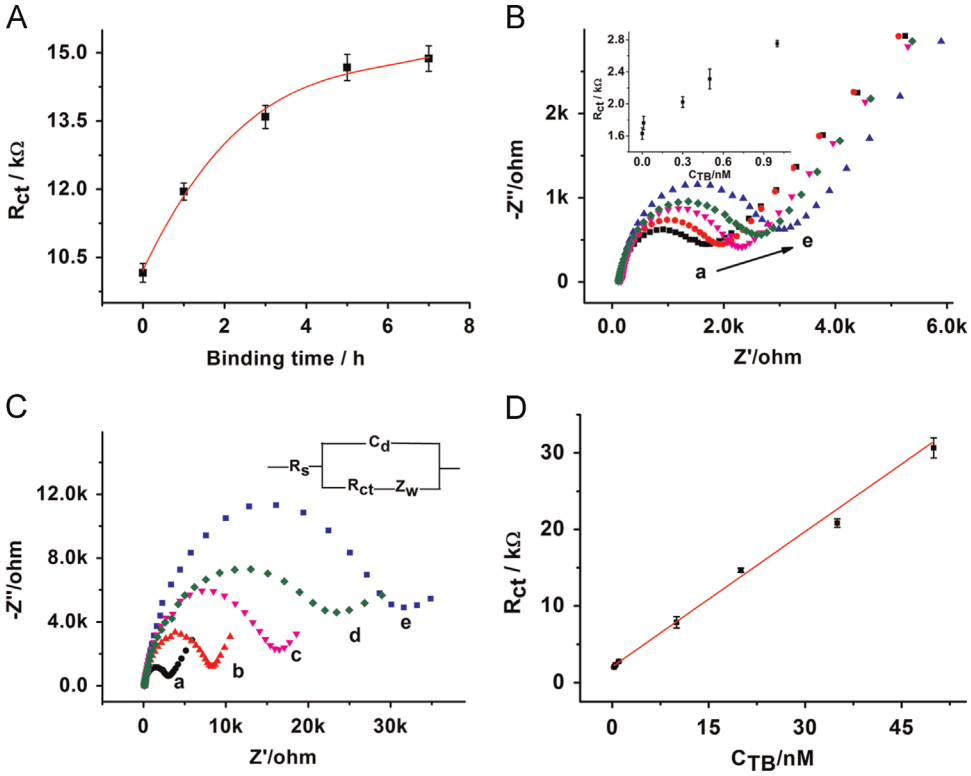

Fig. 5. (A) R_{ct} of rGO–TBA29/TB with different binding time. (B) EIS responses for the detection of different concentrations of TB, from a to e: 0, 0.01, 0.3, 0.5 and 1 nM. Inset: the R_{ct} responses depending on the TB concentrations from 0 to 1 nM. (C) EIS responses for the detection of different concentrations of TB, from a to e: 1, 10, 20, 35 and 50 nM. Inset: the equivalent circuit. (D) The calibration curve of the TB detection. The error bars represent the average standard deviation of three measurements.

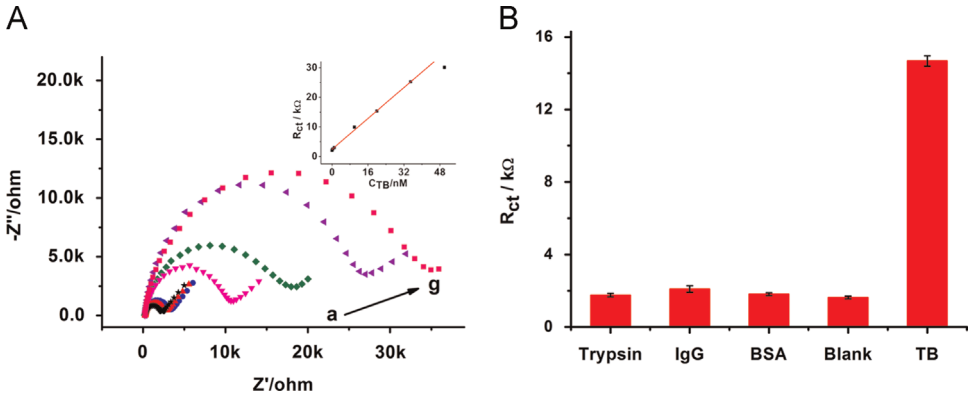

Fig. 6. (A) EIS response of the sensing interface to TB at different concentrations in the 1% fetal calf serum, from a to g: 0, 0.3, 1.0, 10, 20, 35 and 50 nM. Inset: the calibration curve of the TB detection in the diluted serum. (B) Specificity of aptasensor for TB. The R_{ct} values for proteins (trypsin, IgG and BSA) were measured at the same concentration of 1 μM. The concentration of TB was 20 nM.

as 0.01 nM. By using graphene nanocomposites, the EIS signals increased obviously, improving the sensitivity of the biosensor. Without a signal amplified sandwich system, only slight R_{ct} increase could be seen as shown in Fig. 4B. It was significant for the aptasensor to receive an enhanced signal by forming such a sandwich system. All data implied that the as-prepared aptasensor based on the signal amplified sandwich system was not only very simple but also effective for TB detection.

The analytical performance of the aptasensor was evaluated in the diluted serum. In the 1% fetal calf serum, different concentrations of TB were detected by the EIS measurement. The results were shown in Fig. 6A; the impendence was increased with increase of concentration of extrinsic TB. From the inset of Fig. 6A, it was apparent that R_{ct} had a fine linear relationship with the concentration of TB from 0.3 nM to 35 nM. The regression equation was R_{ct} (Ω) = 650.2C_{TB} (nM) + 2505. The results definitely illustrated the potential application of this aptasensor in real samples.

A set of control experiments was also carried out to investigate the specificity of this system. Three kinds of proteins (BSA, IgG and trypsin) were chosen as controls to explore the selectivity of the sensor. As presented in Fig. 6B, compared with blank, TB obtained an amplified signal after incubating with rGO–TBA29. However, the response signals of controls hardly changed, which were much lower than that of TB. This meant that three kinds of proteins could not interact with the TBA15 and interfere the detection of TB. Therefore, all results implied that label-free aptasensor offered high selectivity toward TB.

4. Conclusions

A novel functionalized graphene nanocomposite (rGO–AuNPs) was prepared as an excellent signal amplified platform for TB detection. Hundreds of TBA29 could covalently bind to the AuNPs which were largely absorbed on the surface of rGO, resulting in a high sensitivity to TB. Accordingly, a label-free electrochemical impedimetric aptasensor based on a signal amplified sandwich system was fabricated, which showed an increased response of R_{ct} with the increase of TB concentration from 0.01 nM to 50 nM and the linear range is from 0.3 nM to 50 nM. In addition, AuNPs and graphene could also be labeled with other probes via electrostatic or π–π stacking interactions to produce signals, the model designed here provides a promising application for the detection of other molecules.

Acknowledgments

This work was supported by the National Natural Science Foundation of China (No. 21375123), and 973 Project (No. 2010CB933603).

References

[1] J.D. Roy-Mayhew, D.J. Bozym, C. Punckt, I.A. Aksay, ACS Nano 4 (2010) 6203–6211.
[2] H. Gwon, H.-S. Kim, K.U. Lee, D.-H. Seo, Y.C. Park, Y.-S. Lee, B.T. Ahn, K. Kang, Energy Environ. Sci. 4 (2011) 1277–1283.
[3] J. Zhao, G. Chen, L. Zhu, G. Li, Electrochem. Commun. 13 (2011) 31–33.
[4] W. Wen, T. Bao, J. Yang, M.-Z. Zhang, W. Chen, H.-Y. Xiong, X.-H. Zhang, Y.-D. Zhao, S.-F. Wang, Sens. Actuators B: Chem. 191 (2014) 695–702.
[5] H. Zhang, S. Shuang, L. Sun, A. Chen, Y. Qin, C. Dong, Microchim. Acta 181 (2014) 189–196.
[6] M. Zhou, Y. Zhai, S. Dong, Anal. Chem. 81 (2009) 5603–5613.
[7] F. Liu, Y. Zhang, J. Yu, S. Wang, S. Ge, X. Song, Biosens. Bioelectron. 51 (2014) 413–420.
[8] Z. Zhang, S. Liu, Y. Shi, Y. Zhang, D. Peacock, F. Yan, P. Wang, L. He, X. Feng, S. Fang, J. Mater. Chem. B 2 (2014) 1530–1538.
[9] H. Chang, L. Tang, Y. Wang, J. Jiang, J. Li, Anal. Chem. 82 (2010) 2341–2346.
[10] Y. Wang, Z. Li, D. Hu, C.-T. Lin, J. Li, Y. Lin, J. Am. Chem. Soc. 132 (2010) 9274–9276.
[11] H. Dong, W. Gao, F. Yan, H. Ji, H. Ju, Anal. Chem. 82 (2010) 5511–5517.
[12] X. Sun, F. Li, G. Shen, J. Huang, X. Wang, Analyst 139 (2014) 299–308.
[13] S. Guo, D. Wen, Y. Zhai, S. Dong, E. Wang, ACS Nano 4 (2010) 3959–3968.
[14] M. Famulok, G. Mayer, M. Blind, Acc. Chem. Res. 33 (2000) 591–599.
[15] S.D. Jayasena, Clin. Chem. 45 (1999) 1628–1650.
[16] S. Tombelli, M. Minunni, M. Mascini, Biosens. Bioelectron. 20 (2005) 2424–2434.
[17] C. Tuerk, L. Gold, Science 249 (1990) 505–510.
[18] M. Citartan, S.C.B. Gopinath, J. Tominaga, S.-C. Tan, T.-H. Tang, Biosens. Bioelectron. 34 (2012) 1–11.
[19] M. Ewles, L. Goodwin, Bioanalysis 3 (2011) 1379–1397.
[20] M. Famulok, J.S. Hartig, G. Mayer, Chem. Rev. 107 (2007) 3715–3743.
[21] J. Liu, M. You, Y. Pu, H. Liu, M. Ye, W. Tan, Curr. Med. Chem. 18 (2011) 4117–4125.
[22] I. Willner, M. Zayats, Angew. Chem. Int. Ed. 46 (2007) 6408–6418.
[23] P. He, L. Liu, W. Qiao, S. Zhang, Chem. Commun. 50 (2014) 1481–1484.
[24] Q. Chen, W. Tang, D. Wang, X. Wu, N. Li, F. Liu, Biosens. Bioelectron. 26 (2010) 575–579.
[25] T. Hianik, V. Ostatna, Z. Zajacova, E. Stoikova, G. Evtugyn, Bioorg. Med. Chem. Lett. 15 (2005) 291–295.
[26] Y. Bai, F. Feng, L. Zhao, C. Wang, H. Wang, M. Tian, J. Qin, Y. Duan, X. He, Biosens. Bioelectron. 47 (2013) 265–270.
[27] Q. Yue, T. Shen, L. Wang, S. Xu, H. Li, Q. Xue, Y. Zhang, X. Gu, S. Zhang, J. Liu, Biosens. Bioelectron. 56 (2014) 231–236.
[28] Y. Lv, Q. Xue, X. Gu, S. Zhang, J. Liu, Analyst 139 (2014) 2583–2588.
[29] C.-K. Chen, C.-C. Huang, H.-T. Chang, Biosens. Bioelectron. 25 (2010) 1922–1927.
[30] L. Deng, Y. Du, J.-J. Xu, H.-Y. Chen, Biosens. Bioelectron. 59 (2014) 58–63.
[31] Q. Chen, H. Chen, Y. Zhao, F. Zhang, F. Yang, J. Tang, P. He, Biosens. Bioelectron. 54 (2014) 547–552.
[32] F.-Y. Yeh, T.-Y. Liu, I.H. Tseng, C.-W. Yang, L.-C. Lu, C.-S. Lin, Biosens. Bioelectron. 61 (2014) 336–343.

[33] Y. Wu, W. Xu, L. Bai, Y. Yuan, H. Yi, Y. Chai, R. Yuan, Biosens. Bioelectron. 50 (2013) 50–56.
[34] S. Liu, X. Xing, J. Yu, W. Lian, J. Li, M. Cui, J. Huang, Biosens. Bioelectron. 36 (2012) 186–191.
[35] Y. Du, C. Chen, J. Yin, B. Li, M. Zhou, S. Dong, E. Wang, Anal. Chem. 82 (2010) 1556–1563.
[36] C.-Y. Lee, K.-Y. Wu, H.-L. Su, H.-Y. Hung, Y.-Z. Hsieh, Biosens. Bioelectron. 39 (2013) 133–138.
[37] S. Hu, G. Xi, H. Jin, Y. He, R.F. Keep, Y. Hua, Brain Res. 1424 (2011) 60–66.
[38] Y. Wang, R. Yuan, Y. Chai, Y. Yuan, L. Bai, Biosens. Bioelectron. 38 (2012) 50–54.
[39] W.S. Hummers, R.E. Offeman, J. Am. Chem. Soc. 80 (1958) 1339.
[40] Z. Zhang, H. Chen, C. Xing, M. Guo, F. Xu, X. Wang, H.J. Gruber, B. Zhang, J. Tang, Nano Res. 4 (2011) 599–611.
[41] B.L. Li, Y.L. Wang, H. Wei, S.J. Dong, Biosens. Bioelectron. 23 (2008) 965–970.
[42] H. Qi, S. Li, C. Li, X. Li, Q. Gao, C. Zhang, Biosens. Bioelectron. 39 (2013) 324–328.
[43] S. Campuzano, F. Kuralay, M.J. Lobo-Castanon, M. Bartosik, K. Vyavahare, E. Palecek, D.A. Haake, J. Wang, Biosens. Bioelectron. 26 (2011) 3577–3583.
[44] D. Xu, D. Xu, X. Yu, Z. Liu, W. He, Z. Ma, Anal. Chem. 77 (2005) 5107–5113.
[45] C.-Z. Li, Y. Liu, J.H.T. Luong, Anal. Chem. 77 (2004) 478–485.